Experimental energy band dispersions and lifetimes for valence and conduction bands of copper using angle-resolved photoemission

J. A. Knapp, F. J. Himpsel, and D. E. Eastman
IBM Thomas J. Watson Research Center, Yorktown Heights, New York 10598
(Received 18 September 1978)

Energy-band dispersions and electron lifetimes have been determined for both valence and conduction-band states of copper using angle-resolved photoemission with polarized synchrotron radiation in the $5 \leq h\nu \leq 35$ eV photon energy range. Dispersion relations for the occupied s-p and $3d$ bands of Cu along the Γ-X and Γ-L symmetry lines (including critical points at Γ, X, and L) have been determined with an accuracy of 0.05–0.1 eV and $\lesssim 5\%$ of the zone-boundary momentum. Band symmetries have been deduced using polarization selection rules. The dispersion relation has also been accurately determined for the unoccupied Δ_1 conduction band along Γ-X at $\sim$10–15 eV above the Fermi energy E_F; this band has a reduced effective mass ($m^* \simeq 0.90$–0.94) which is related to self-energy effects. Lifetimes have been directly measured for excited hole states (the lifetime broadening Γ_h increases from $\sim$0.2 to 0.5 eV full width at half maximum for d-band energies from 2 to 5 eV below E_F) as well as for excited electron states in the Δ_1 conduction band ($\Gamma_e \simeq 1.0$–2.0 eV for energies 10–15 eV above E_F). The energy dispersion and $h\nu$-dependent photoionization cross section of the s-p surface state on Cu(111) are reported. Previous theoretical and experimental studies of copper are compared with our accurate E vs $\vec{k}$ dispersions.

I. INTRODUCTION

Angle-resolved photoemission (ARPES) from single-crystal copper has been studied by several workers.[1-9] The continued interest in copper is due to its place as an ideal theoretical and experimental testing ground for our understanding of the electronic structure and various excitation processes of nonsimple materials, i.e., materials containing d electrons. It is nonmagnetic and its band structure can be well described by nonrelativistic calculations. It has been shown that photoemission data can be successfully interpreted in terms of the three-step model[10] of photoemission including conservation of energy and momentum during the excitation process.[3,7,8,11] The use of a three-step direct transition model permits an experimental mapping of the energy versus momentum (E vs k) dispersion relations,[3,7,8,12] which gives a fundamental description of the electronic structure. Of particular interest are E vs k dispersions along high-symmetry lines of momentum space,[7,8] since these can be most easily related to theoretical models, and thus to other physical properties. Since the photoexcitation involves both the initial- and final-band energies and momenta, an accurate mapping of the initial bands requires a reasonable knowledge of the final bands involved. Recent studies of copper in the photon energy range above 30 eV simply used the empty-lattice free-electron band structure for the final state.[7,8,11] In this paper, we have used a variant of this procedure as well as other angle-resolved photoemission techniques to obtain accurate descriptions of energy-band dispersions as well as values of electron-hole lifetimes for excited valence- and conduction-band states in copper. We use normal-emission data from Cu(100) and Cu(111) for photon energies ($5 \leq h\nu \leq 35$ eV) together with calculated final bands from a two-parameter self-consistent calculation (by Janak, Williams, and Moruzzi[13]), which was fit to Fermi-surface and optical data and which had previously been found to provide a good description of angle-averaged photoemission data. The use of these calculated final bands, combined with good energy and angular resolution and the smaller inherent final-state momentum broadening at lower energies, has permitted us to map out the initial s-p and $3d$ band structure along the $\Gamma\Lambda L$ and $\Gamma\Delta X$ symmetry lines much more accurately and completely than has previously been possible.

An outline and brief summary of this paper is as follows. In Sec. II we describe experimental procedures. In Sec. III we describe angle-resolved photoemission techniques and data for Cu(111) and Cu(100) which have been used to determine the E vs k dispersions for occupied s-p and d bands along $\Gamma\Lambda L$ and $\Gamma\Delta X$. In Sec. IV, we describe techniques and data which have been used to accurately determine E vs k dispersion relations for portions of the lowest unoccupied conduction bands along Λ and Δ. Comparison of our experimentally determined bands with theory indicates the existence of significant self-energy effects. In Sec. V we describe measurements of hole lifetimes for the $3d$ bands of Cu as well as lifetimes of electrons excited into the Δ_1 conduction band at

~10–14 eV above E_F. Average $3d$ hole lifetimes are found to increase in energy from $\Gamma_h \simeq 0.2$ eV at the top of the d bands to $\Gamma_h \simeq 0.5$ eV at the bottom of the d-bands full width at half maximum (FWHM). Lifetimes of excited electron states are found to increase in energy from $\Gamma_e \sim 1$ eV at 10 eV above E_F to ~2 eV at 14 above E_F. Energy-dependent electron mean free paths and momentum broadenings for the noble metals in the 5–70 eV range are summarized. In Sec. VI, $h\nu$-dependent relative photoionization cross section measurements and the E vs k dispersion relation for the s-p surface state on Cu(111) are described. No final-state resonances in the cross section have been observed for $8 \leq h\nu \lesssim 25$ eV. In Sec. VII, a comparison of our E vs k dispersion relations with the results of various theoretical models and past experiments is presented.

II. EXPERIMENTAL PROCEDURE

The light source for these measurements was synchrotron radiation from the 240-MeV electron storage ring at the University of Wisconsin's Synchrotron Radiation Center. The samples were studied in two different photoemission spectrometers in order to optimize the range of available radiation polarizations. For measurements with nearly pure s polarization, a double-pass cylindrical mirror analyzer (CMA) was used which has been modified for angle-resolved electron spectroscopy by means of an internal aperture.[14] The CMA was operated with angular resolution $\delta\theta = 4°$ and a total energy resolution of ~150 meV (photons plus electrons). For measurements with strongly p-polarized radiation, a new two-dimensional display-type spectrometer was used. An angle-resolving aperture selected a cone of $\delta\theta \simeq 4°$ from the total acceptance cone of the analyzer (1.8 sr). The total energy resolution for this second spectrometer was ~100 meV. With typical storage-ring beam currents, the count rates for the Cu d bands were about 10^4 counts/sec (both spectrometers).

Clean Cu(100) and Cu(111) crystals were prepared in each chamber by argon sputtering and annealing to $\lesssim 600$ °C and checked for cleanliness using Auger electron spectroscopy. The working vacuums were less than 1×10^{-10} Torr for both chambers. At these pressures, the samples showed no significant contamination for at least several hours.

III. ENERGY VERSUS MOMENTUM DISPERSION RELATIONS FOR OCCUPIED BANDS

We show in Figs. 1–5 angle-resolved photoemission energy distribution curves (AREDC's) obtained at normal emission from Cu(100) and Cu(111). Collecting spectra at normal emission considerably simplifies the analysis of the results. Conservation[15] of the component of the electron's momentum parallel to the surface, $\vec{k}_s$, implies that electrons collected normal to the surface ($\vec{k}_s = 0$) originate along a line in k space inside the crystal defined by $\vec{k}_s = 0$. For samples prepared with their crystal faces parallel to low-index planes, the AREDC data is directly related to the band structure along selected high-symmetry lines in the bulk Brillouin zone (BZ), e.g., the $\Gamma\Lambda L$ line for Cu(111) and the $\Gamma\Delta X$ line for Cu(100). An additional advantage rests on the fact that emission from surface states is fixed in initial energy at constant $\vec{k}_s$. Thus for normal emission, peaks due to surface states will show no dispersion in initial energy as a function of photon energy.

The advantages of studying the normal emission are illustrated in Fig. 1. Several AREDC's taken at normal emission from Cu(111) for photon energies $6 \leq h\nu \leq 11.5$ eV are shown, plotted versus initial energy below the Fermi level E_F. The peak at $E_i = -0.4$ eV in all curves is due to a surface state, which is common to the (111) faces of Cu, Ag, and Au.[4,16,17] Clearly, this peak is the only feature that does not show dispersion as a function of photon energy. The structure near $E_i = -2.5$ eV in each spectrum is due to the $3d$ band of Λ_3 sym-

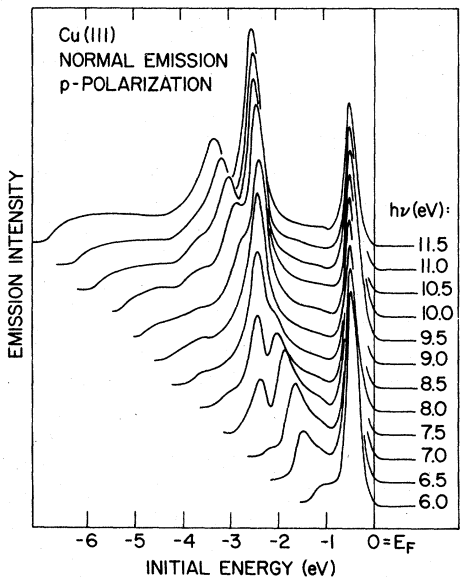

FIG. 1. Normal-emission AREDC's obtained from Cu(111) using p-polarized light at photon energies $6.0 \leq h\nu \leq 11.5$ eV, showing several direct transition bulk emission peaks as well as emission from an sp-like surface state at initial energy $E_i = -0.4$ eV.

metry along the Λ line in the bulk BZ, while the feature which moves from $E_i = -1.5$ eV at $h\nu = 6.5$ eV to $E_i = -3.3$ eV at $h\nu = 11.5$ eV is due to transitions from the s-p band of Λ_1 symmetry. A detailed analysis of these peak positions to determine the initial E vs k dispersion will be presented. The orientation of the optical electric field $\vec{E}$ was such that the radiation was ~90% p polarized ($\vec{E}$ parallel to the plane of incidence) for the spectra of Fig. 1. Figure 2 shows another set of AREDC's for Cu(111) which continue from $h\nu = 12$ eV up to $h\nu = 30$ eV at an orientation where the radiation was ~60% p polarized. The magnitude of the surface-state emission decreases dramatically at higher photon energies, relative to the d-band emission. Emission from the d bands along Γ exhibits intensity modulation and dispersion throughout the photon energy range.

Three pairs of AREDC's at $h\nu = 12$, 20, and 26 eV shown in Fig. 3 display the polarization dependence of the principle features in Cu(111) normal emission. The solid curves were obtained with ~90% p polarization, while the dashed curve of each pair was obtained using radiation of ~75% s polarization. The dependence of emission intensity on the orientation of $\vec{E}$ with respect to the crystal is a useful tool for determining the symmetries of the electronic wave functions involved in the transition. Hermanson[18] has shown that for $\vec{k}_s = 0$ (normal emission) the final state must be totally symmetry under point-group operations about the normal, implying that the initial-state symmetry is given by the symmetry of the dipole operator $\vec{E} \cdot \vec{\nabla}$. For the Γ-Λ-L line, only initial states of symmetry Λ_3 (e.g., $p_{x,y}$, d_{xy}) and Λ_1 (e.g., s, p_z) are allowed, with Λ_3 excited by the component of $\vec{E}$ parallel to the surface and Λ_1 excited by the component perpendicular to the surface. In Fig. 3, the surface-state emission is clearly stronger for p-polarized light; therefore it has Λ_1 symmetry. The three pairs of AREDC's are normalized to the middle peak (Λ_3 symmetry); this emphasizes those features which have Λ_1 symmetry. The lowest peak at $h\nu = 12$ eV and $h\nu = 20$ eV is clearly Λ_1 in character, while at $h\nu = 26$ eV the symmetry is predominantly Λ_3.

Normal-emission data taken for the Cu(100) face are shown in Figs. 4 and 5. Normal emission from this face samples the Γ-Δ-X line, from which only states of Δ_1 and Δ_5 symmetry are allowed by the selection rules,[18] for p and s polarization, respectively. Other symmetries, e.g., Δ_2 or Δ_2', are not allowed for normal emission. Figure 4

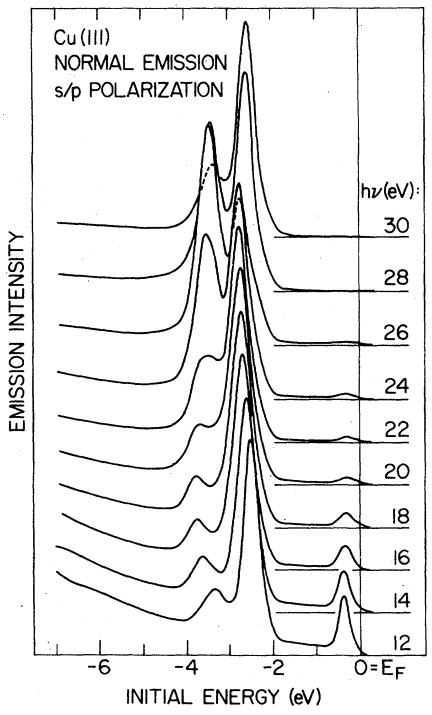

FIG. 2. Normal-emission AREDC's obtained from Cu(111) for photon energies $12 \leq h\nu \leq 30$ eV.

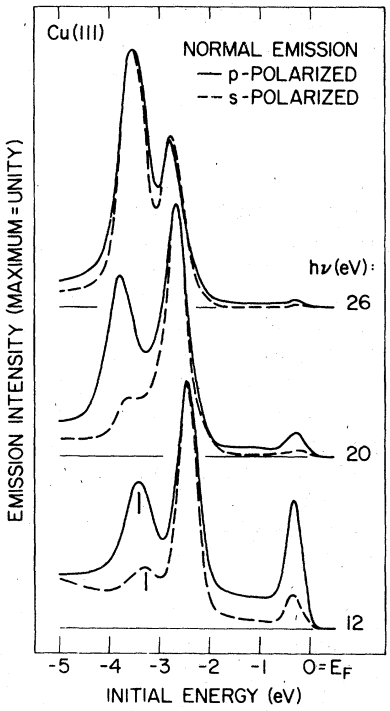

FIG. 3. Three pairs of normal-emission AREDC's obtained from Cu(111) at $h\nu = 12$, 20, and 26 eV, showing the polarization dependence of several emission features. The dashed curve of each pair was obtained with s-polarized light, the solid curve with p-polarized light.

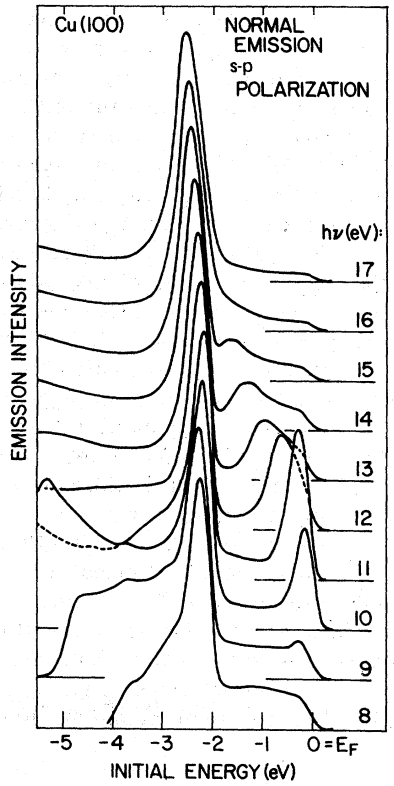

FIG. 4. Normal emission AREDC's obtained from Cu(100) with mixed polarization at photon energies $8 \leq h\nu \leq 17$ eV, showing direct transitions from the sp band between E_F and the d bands at $E_i = -2$ eV.

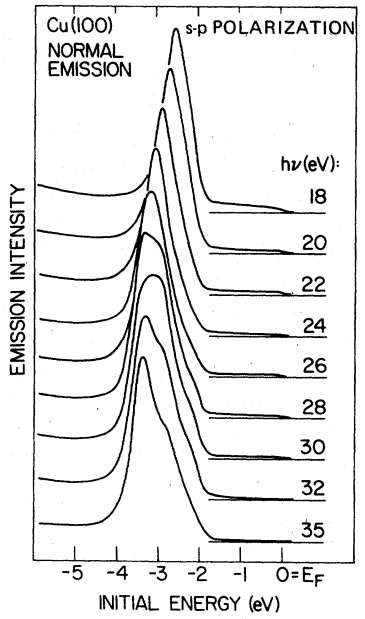

FIG. 5. Normal emission AREDC's obtained from Cu(100) for photon energies $18 \leq h\nu \leq 35$ eV.

shows AREDC's from $h\nu = 8$ eV to 17 eV, taken with mixed polarization (~60% p polarized). There are two features in the spectra: (a) Emission from the d band of Δ_5 symmetry near $E_i \sim 2.5$ eV in each AREDC, and (b) emission from the s-p band of Δ_1 symmetry, which disperses from E_F at threshold ($h\nu = 10.6$ eV) down to coincidence with the d band at $h\nu \simeq 16$ eV. The $h\nu$-dependent onset and linewidth of the s-p band transition at E_F are related to the lifetime of the final state involved (see Sec. V). Emission spectra for higher photon energies are illustrated in Fig. 5. The main peak (d band and s-p band) disperses to lower initial energy and then changes character to that of a doublet or triplet above $h\nu \simeq 26$ eV. As we will show in connection with Fig. 6, this corresponds to the onset of emission into multiple final bands.

To obtain bulk energy band dispersions from the observed interband transitions, we use a calculated nearly-free-electron-like final band. Previous interpretations of data taken from these faces of Cu at higher photon energy used a completely free-electron-like final band shifted only by a constant inner potential.[7,8,11] Our approach of using calculated bands for the final state is necessary at the lower photon energy range ($h\nu \lesssim 35$ eV), due to non-free-electron-like effects (e.g., the presence of the d-band resonance), and is inherently a more accurate way of determining the initial bands. Furthermore, our data are more accurate due to decreased k broadening (i.e., larger escape depth,[19] see Sec. V), better angular resolution, and better energy resolution, all of which occur at lower photon energy. Finally, the influence of umklapp induced final bands, compared to the primary nearly-free-electron band, has not been assessed yet for the higher photon energies.

The energy bands we have used in the data interpretation were calculated by Janak, Williams, and Moruzzi (JWM) using a two-parameter self-consistent theory.[13] The first parameter, the exchange coefficient α appearing in Slater's $X\alpha$ theory, was adjusted such that the ground-state energy bands described the measured Fermi surface.[20] The second parameter λ, which describes the self-energy contribution appearing in the Sham-Kohn local-density theory of excitations, was adjusted to optical-absorption and angle-integrated ultraviolet-photoemission-spectroscopy (UPS) data.[18] The band structure was found to reproduce the previous data most accurately for $\alpha = 0.77$ and $\lambda = 0.08$. It should be noted that this band calculation was not fitted to the angle-resolved UPS data that we are presenting here, but that it nonetheless accurately matches our results.

Experimental energy versus momentum dispersions for the initial energy bands of Cu along Γ-Λ-L and Γ-Δ-X are summarized in Fig. 6. Experimental points were plotted using the data exemplified by Figs. 1–5 and Λ_1 and Δ_1 calculated final bands along the respective symmetry lines. The energy scale at the top of Fig. 6 indicates the experimental final energy. The initial energy relative to the Fermi level is obtained directly from the AREDC with a typical relative accuracy of 0.05 eV. The magnitude of $\vec{k}$ is determined by assuming a direct transition to the calculated final band of final energy $E_f = h\nu + E_i$, where $h\nu$ is the photon energy and E_i is the initial energy relative to E_F. For the Γ-Λ-L line, only one final band is available from threshold up to ~23 eV above E_F (see Fig. 16); above this energy, transitions to a second band are allowed as well. Along the Γ-Δ-X line, a single final band is available for energies up to ~14.6 eV above E_F. Above these energies, a peak in the AREDC could be assigned to either of two final bands, giving two values of k. The regions of k space for which these ambiguities exist are lightly crosshatched, although transitions to these secondary bands (secondary cones, in Mahan's[46] terminology) proved to be generally weaker than to the primary bands. The data were not used to plot the initial bands at higher final energies ($E_i \gtrsim 25$ eV) because of these ambiguities and because of difficulties in separating closely spaced emission features.

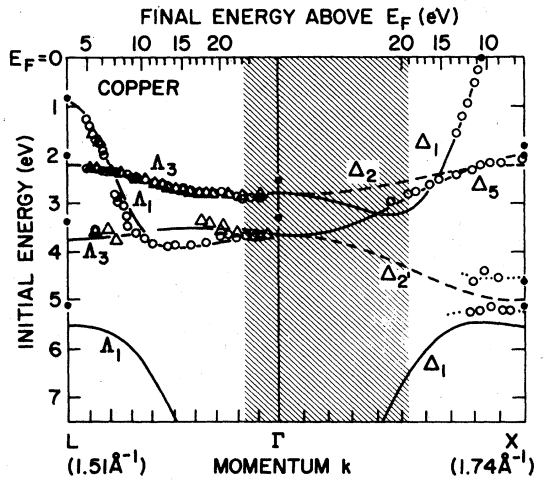

FIG. 6. Experimentally determined initial-band dispersions (E vs k) for copper along the $\Gamma\Lambda L$ and $\Gamma\Delta X$ symmetry lines. The experimental points are obtained as described in the text. Open circles correspond to s-p polarization, open triangles to s polarization. The solid and dashed lines are from an $X\alpha$ calculation obtained with an 8% self-energy stretch (Ref. 13). The solid dots at L, Γ, and X correspond to energies of the $X\alpha$ calculation without the self-energy adjustment (Ref. 20).

The calculated bands indicated in Fig. 6 are due to JWM.[13] Solid bands are of symmetries which are allowed for transitions with normal emission; dashed bands are not allowed. Also indicated in Fig. 6 by solid dots at the symmetry points and E_F are the critical-point energies calculated using $\alpha = 0.77$ but with no self-energy correction[20]; this calculation clearly places the d bands too high in energy. The calculation using the self-energy correction[13] is in good agreement (generally within 0.1 eV, except the lower bands at X) with our experimental band plot.

IV. ENERGY VERSUS MOMENTUM DISPERSION RELATIONS FOR UNOCCUPIED BANDS

The accuracy with which the experimental value of $\vec{k}$ may be determined for the initial bands is limited by the accuracy of the calculated final bands. For special cases, information about the energy position and dispersion of final bands can be obtained directly from the photoemission data. The final bands of interest are shown in Fig. 7. The dispersion of a portion of the Δ_1 band may be determined from the data, since the dispersion of the initial band along Δ near E_F is accurately known from analyses of the de Haas–van Alphen Fermi-surface data together with Cu d-band photoemission data.[13,20] Namely, the $X\alpha$ and combined interpolation scheme calculations agree within ~0.02 eV and 0.01 Å^{-1} for initial Δ_1 states within ~1.5 eV of E_F. By using this known initial-state s-p-band dispersion, portions of the final bands may be plotted in the same way as the calculated final bands were used to plot the initial d bands in Fig. 6. Figure 7 illustrates the procedure and displays the results. The lower part of the figure shows those portions of the calculated s-p bands which are between E_F and the $3d$ bands for the regions of k space near L and X. In the upper part of Fig. 7 are plotted the experimental points obtained by assuming that the lower s-p band is correct. The final energy above E_F for each point is $E_F = h\nu + E_i$, where E_i is the initial energy of the s-p band emission peak, and k is determined from the initial band calculated by JWM.[13] For the Λ direction the calculated initial band is expected to be accurate in the region we have used it, i.e., away from the zone boundary; however, there is no definitive check of this accuracy such as given by Fermi-surface data for the Δ_1 band.

Comparison of our experimentally determined Δ_1 and Λ_1 conduction bands in Fig. 7 with calculated bands shows excellent agreement with the $X\alpha$ calculation[13] ($\alpha = 0.77$, $\lambda = 0.08$). Comparison (not

shown) with the combined interpolation scheme mode,[22] which relied on fitting to the conduction bands of an augmented-plane-wave (APW) calculation,[23] shows that the calculated Δ_1 band and higher-lying Λ_1 band lie too low in energy. This is consistent with the $X\alpha$ calculation, which gives a very similar result if the 8% self-energy factor mass (i.e., $\lambda = 0.08$) is omitted.[20] We have also fit experiment with a simple two-OPW (orthogonalized-plane-wave) model (not shown) and compared various calculated effective masses with that determined from experiment using the relation $\partial E/\partial k = 7.62k/m^*$ and the experimental average group velocity of $\partial E/\partial k = 1.72 \pm 0.2$ eV Å for energies between 11 and 14 eV above E_F. These comparisons indicate that an effective mass of $m^* = 0.90$–0.94 is needed to fit the Δ_1 conduction-band dispersion (in agreement with the $X\alpha$ calculation with $\lambda = 0.08$, i.e., $m^* = 0.92$). This effective mass is significantly less than unity and indicates the existence of important self-energy effects.[13]

We have also determined the X_1 critical point of the Δ_1 conduction band, which lies above the vacuum level ϕ. Figure 8 summarizes two different types of experimental spectra for Cu(100) which indicate the position of the X_1 point. In Fig. 8(a), the maximum of the d-band peak emission at $E_i \simeq -2.0$ eV (Δ_5 near X_5), normalized to the incident light flux, is plotted versus final energy above E_F (obtained at discrete photon energies $7.5 \leq h\nu \leq 11.5$ eV). The arrow at $E_f = 7.9$ eV corresponds with a change in slope of the emission intensity. D-band emission below this energy (i.e., at lower photon energy) is due to transitions into evanescent final states near the surface; the change of slope at $E_f \sim 7.9$ eV corresponds to the onset of direct transitions into the Δ_1 final band, i.e., the X_1 critical point.

In Fig. 8(b), the low-kinetic-energy portions of normal-emission AREDC's from both Cu(100) and Cu(111) are plotted versus final energy above E_F. These portions of the AREDC's [with $h\nu = 17$ eV for Cu(100) and 16 eV for Cu(111)] are due to secondary electron emission, and are expected to reflect structure in the one-dimensional densities of final states along Δ and Λ, respectively. As in Fig. 8(a), the curve for Cu(100) shows a distinct change in slope at $E_F \sim 7.9$ eV, which reflects the presence

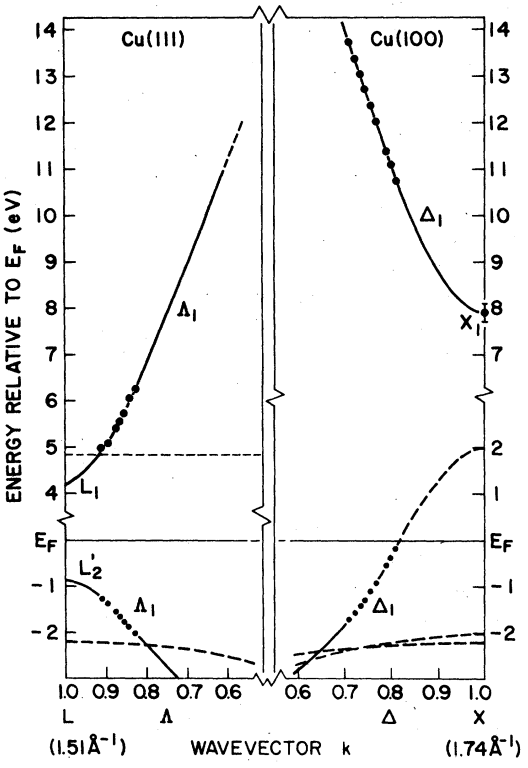

FIG. 7. Experimentally determined final-band dispersions (E vs k) for portions of the lower Λ_1 and Δ_1 bands in copper. Only a portion of each symmetry line is shown, and the energy scale is broken for convenience. The dots are determined from the data as described in the text. The solid lines are from an $X\alpha$ calculation obtained with an 8% self-energy stretch (Ref. 13).

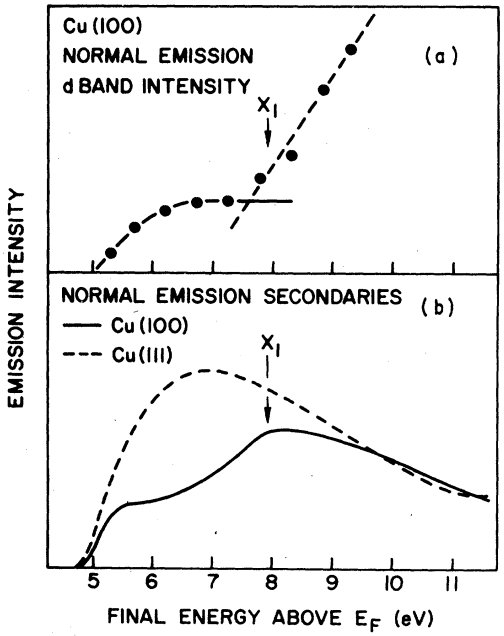

FIG. 8. (a) Emission intensity of the upper d-band peak in Cu (100) normal emission, normalized to the incident photon flux and plotted vs final energy above the Fermi energy E_F. The arrow indicates the energy of the Δ_1 band minimum at X_1. (b) Low-energy portions of normal emission AREDC's from Cu(100) and Cu(111), obtained at $h\nu = 17$ eV and 16 eV, respectively, also plotted vs final energy.

of the X_1 band minimum. The AREDC for Cu(111), on the other hand, has no such structure, only a typically smooth distribution of scattered electrons. Above the X_1 point, the intensity of scattered electron emission for Cu(100) is a smooth function which decreases [relative to the analogous Cu(111) distribution] as the energy approaches $E_f \sim 7.9$ eV from above. This behavior reflects the decrease in escape depth as the final state approaches the band minimum at X_1 (due to the decrease in group velocity). Below $E_f \sim 7.9$ eV, the distribution changes character to a more rapidly decreasing function, reflecting the square-root energy dependence of the imaginary part of the wave functions, with a minimum escape depth at the center of the gap below X_1. The AREDC from Cu(111) shows no such structure since the minimum of the Λ_1 final band lies below the vacuum level. The change in slope in the Cu(100) scattered electron distribution of Fig. 8(b) was seen at constant $E_f \sim 7.9$ eV for all photon energies above $h\nu \sim 14$ eV and can clearly be associated with the X_1 point. The data, as represented by Fig. 8, indicate that X_1 is at $E_f = 7.9 \pm 0.2$ eV, in very good agreement with the self-energy corrected $X\alpha$ calculation.[13]

In summary, we find remarkably good agreement between the $X\alpha$ calculation[13] and experimentally determined portions of the Λ_1 and Δ_1 conduction bands. This indicates that the overall calculated conduction bands[13] are quite accurate for final energies $E_f \lesssim 25$ eV. Thus the uncertainty in k for the experimental band structure plot of Fig. 6 is estimated to be less than $\pm 5\%$ of $k_{\mathrm{BZ}}^{\langle 100\rangle}$, the full magnitude of k from Γ to X. This uncertainty is due in part to the final-state momentum broadening due to the short lifetimes of the excited electron states, which will be discussed next.

V. ELECTRON-HOLE LIFETIMES FOR VALENCE- AND CONDUCTION-BAND STATES IN COPPER

The lifetimes of excited valence-band hole states and conduction-band electron states are of fundamental interest since they determine such basic quantities as the energy resolution of electron and optical spectroscopies, the electron mean free path (i.e., spatial escape depth), the momentum resolution of angle-resolved photoemission, etc. For metals, electron-hole lifetimes are usually dominated by inelastic electron-electron interactions[24] that result in lifetimes which are increasingly shorter (i.e., more energy broadening) for energies further away from the Fermi energy E_F.

The energy-dependent lifetimes $\Gamma(E)$ of excited hole states can be directly determined using angle-resolved photoemission. Namely, if sufficient experimental energy and momentum resolution are used and conditions are selected such that interband transitions from various valence bands are separated by more than $\Gamma(E)$, then the widths of observed interband transitions at $(E_i, \vec{k})$ are directly related to the widths of the corresponding hole and electron states. If the hole and electron states have Lorentzian spectral distributions of FWHM $\Gamma_h(E_i)$ and $\Gamma_e(E_F)$, respectively, the observed spectral distribution will be a Lorentzian having a width which is approximately given by

$$\overline{\Gamma} = \left(\Gamma_h + \Gamma_e \left|\frac{\partial E_i/\partial k_z}{\partial E_f/\partial k_z}\right|\right) \Big/ \left(1 - \frac{\partial E_i/\partial k_z}{\partial E_f/\partial k_z}\right),$$

where $\partial E_i/\partial k_z$ and $\partial E_f/\partial k_z$ are the group velocities perpendicular to the surface of the initial and final states and we have used the relation that linewidths add when two Lorentzian functions for two independent broadening mechanisms are convolved.[25] The final-state contribution to $\overline{\Gamma}$, which involves the ratio of the group velocities and vanishes in the limit of flat initial-state bands, can be easily seen using a two-plane-wave model.[26]

Two AREDC's for Cu(100) are shown in Fig. 9 which display the spectral widths $\overline{\Gamma}$ for d-band excitations with various initial-state energies. These transitions are well resolved, with a small background due to inelastic secondary electrons that can be unambiguously accounted for. The widths $\overline{\Gamma}$ shown in Fig. 9 together with additional data for $3d$-band excitations are summarized in Fig. 10. $\overline{\Gamma}(E_i)$ is seen to increase roughly linearly from ~ 0.3 eV at -2 eV to ~ 0.6 eV at -5.3 eV. For the interband transition involved in our measurements ($h\nu = 16$ eV), the final states have lifetimes of $\Gamma_e = 1.5 \pm 0.5$ eV and group velocities of $\partial E_f/\partial k_z \simeq 15$–$20$ eV Å (to be discussed). Since the narrow $3d$ bands have small group velocities, $\partial E_i/\partial k_z \simeq 1$ eV Å (see Fig. 6), the final-state contribution to $\overline{\Gamma}$ is approximately given by

$$\Gamma_e \frac{\partial E_i/\partial k}{\partial E_f/\partial k_z} \simeq 0.1 \text{ eV}.$$

Thus we estimate, after correcting for the instrumental broadening, that $\Gamma_h(E_i) \simeq \overline{\Gamma}(E_i) - 0.1$ eV for $3d$ excitations in Cu, where $\Gamma_h(E_i)$ is given in Fig. 10. In summary, we find that $3d$ hole lifetimes (FWHM energy widths) in Cu increase from $\Gamma_h \simeq 0.2$ eV at the top of the d bands to $\Gamma_h \simeq 0.45$ eV at the bottom. In this estimate (upper bound) of average E-dependent lifetimes, we have not considered $\vec{k}$-dependent effects.

For Cu(100), we have directly determined the energy-dependent lifetime $\Gamma_e(E)$ of Δ_1 conduction-band states in the range of ~10–14 eV above E_F.[25] Normal-emission AREDC's which show the onset

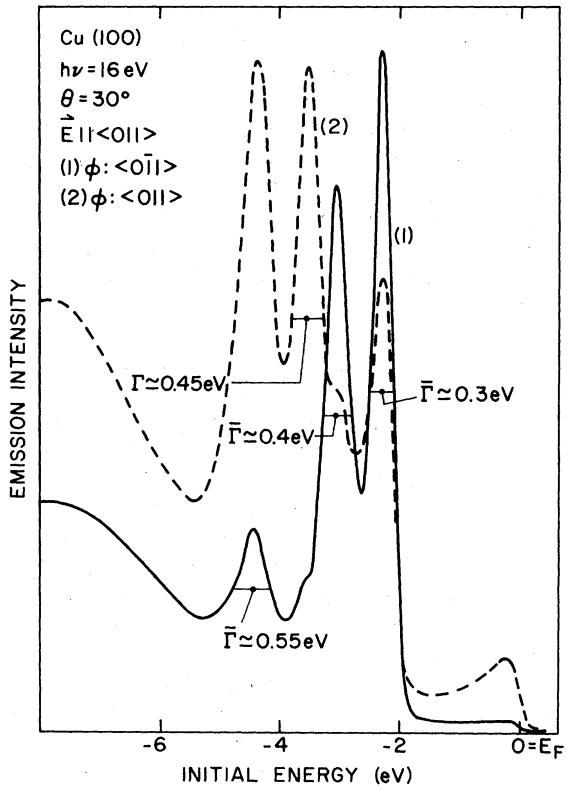

FIG. 9. AREDC's obtained from Cu(100) at $h\nu = 16$ eV at a polar angle $\theta = 30°$ for two crystallographically equivalent azimuths. For curve (1) the collection azimuth is parallel to the $\vec{E}$ vector in the surface, while for curve (2) the collection azimuth is perpendicular to $\vec{E}$. Several d-band transitions are shown, with experimental linewidths indicated.

of interband transitions from the occupied Δ_1 s-p valence band just below E_F into the lowest empty Δ_1 conduction band (e.g., see Fig. 7) are shown in Fig. 11. The vertical dotted lines give the interband transition intensities for excitation from an initial state of energy $E_i = -0.13$ eV. These $h\nu$-dependent interband intensities are summarized

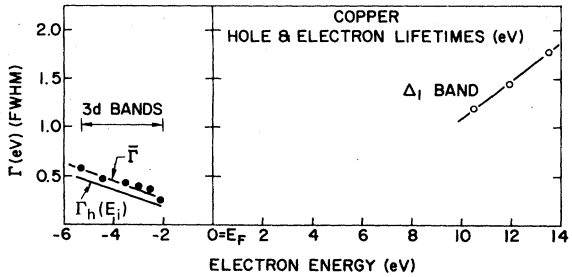

FIG. 10. Experimentally determined hole and electron lifetimes (energy widths) for copper.

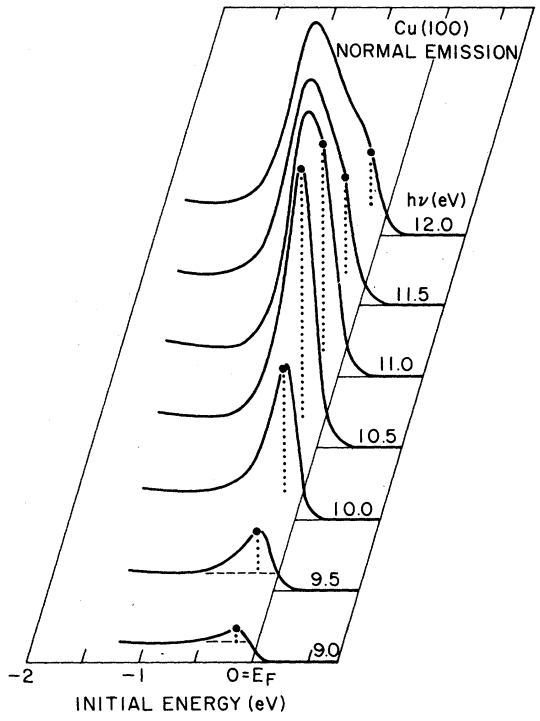

FIG. 11. Normal-emission AREDC's obtained from Cu(100) showing the onset of $\Delta_1 \rightarrow \Delta_1$ interband transitions. The vertical dotted lines depict the interband intensity at an initial energy $E_i = -0.13$ eV.

in Fig. 12. Also shown in Fig. 12 is a Lorentzian function of width $\Gamma = 1.2$ eV and center $h\nu_0 = 10.6$ eV which has been fit to experimental intensities.

We have shown[25] using the three-step model for angle-resolved photoemission that this Lorentzian closely approximates the spectral distribution of the final state, and its width and center energy directly give the lifetime Γ_e and final-state energy

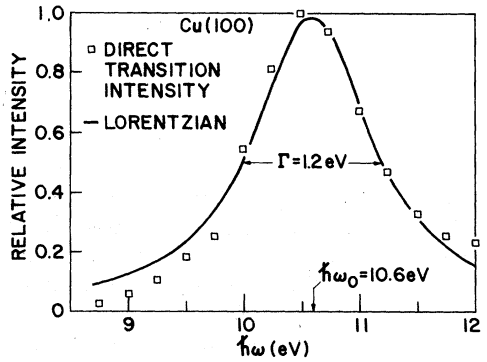

FIG. 12. Interband ($\Delta_1 \rightarrow \Delta_1$) transition intensity vs $h\nu$ for an initial energy $E_i = -0.13$ for normal emission from Cu(100). The theoretical curve is a Lorentzian function of width $\Gamma = 1.2$ eV and center $h\nu_0 = 10.6$ eV.

of the Δ_1 conduction band state at the momenta $k = 0.82 k_{BZ}^{<100>}$ along Δ. This simple result occurs because the various other $h\nu$-dependent factors in the energy-dependent spectral density of the interband transition (e.g., escape probability, interband matrix element, analyzer acceptance) tend to cancel each other and vary much more slowly with $h\nu$ than the spectral distribution of the final state. Also, the initial-state lifetime contribution is negligible since the initial state is very near E_F. Using the above technique, we have determined the energy-dependent lifetimes $\Gamma_e(E)$ shown in Fig. 10 for Δ_1 conduction-band states.

In comparison with past work, the most relevant electron mean-free-path measurements[19] for noble metals for energies $\lesssim 70$ eV appear to be electron transmission measurements for Au and Cu,[27] photoemission escape depth measurements for Ag,[28,29] and Auger escape depth measurements for Ag.[30] These measurements, together with our results for Cu(100), are shown in Fig. 13. Here we have calculated the mean free path $l(E)$ using the relation $l(E) = (\partial E_f/\partial k)/\Gamma_e(E)$, where $\partial E_f/\partial k \simeq 17$ eV Å for the final states involved. The smooth curve for $l(E)$ in Fig. 13 gives our best estimate of the average energy-dependent electron mean free path for the noble metals, based on available data. The noble metals have much longer $l(E)$'s at low energies, (e.g., $E \lesssim 10$ eV) than the transition metals.[19]

Also shown in Fig. 13 are curves for the average energy-dependent momentum broadening (FWHM), $\Delta k = 1/l(E)$, and average energy-dependent energy broadening $\Gamma_e(E)$ for the noble metals. Here we have used $l(E)$ in Fig. 13 and the relation $\Gamma_e(E) = (\partial E_f/\partial k)/l(E)$, with $\partial E_f/\partial k$ given by a free-electron model, $E_f = 3.81k^2 - 6$ eV. Accuracies for $l(E)$, $\Delta k(E)$, and $\Gamma(E)$ in Fig. 13 are estimated to be roughly ±25%. For $E \gtrsim 40$ eV, $\Gamma(E)$ in Fig. 13 is comparable to values for Ni based on a low-energy electron-diffraction (LEED) analysis of diffraction peak lineshapes.[31] It is seen in Fig. 13 for energies $E \lesssim 20$ eV that the momentum broadening is $\Delta k \lesssim 0.1$ Å^{-1}, i.e., $\lesssim 5\%$ of the Brillouin-zone momentum for the noble metals. This momentum broadening, which becomes greater at higher energies, places a fundamental limit on the momentum resolution in angle-resolved photoemission measurements of E vs k dispersion relations such as presented in Sec. III.

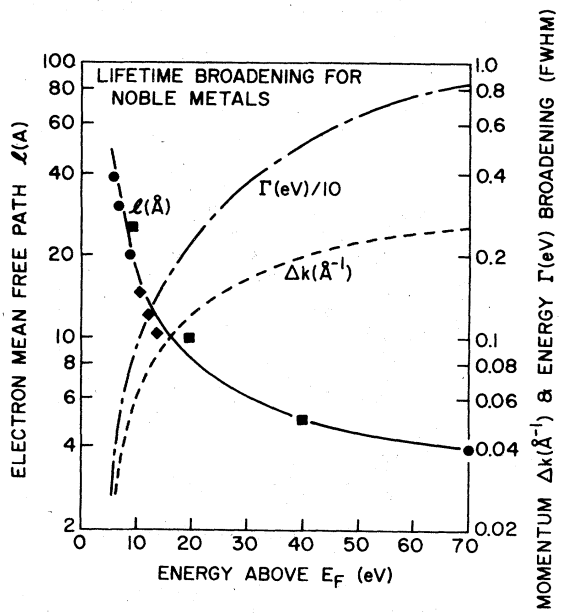

FIG. 13. Experimental energy-dependent energy width (lifetime) $\Delta(E)$, electron mean free path $l(E)$, and momentum broadening $\Delta k(E)$ for the noble metals. ■, Ref. 28; ●, Refs. 27 and 30; ♦, present data.

VI. CU (111) SURFACE STATE

One very dramatic feature seen for normal emission from Cu(111) at lower photon energies for p-polarized light is the surface-state emission at $E_i = -0.4$ eV in Figs. 1 and 2. This sp-like surface state lies in the Λ_1 symmetry gap above L_2', and was first identified by Gartland and Slagsvold.[4] Similar surface states have been reported for the (111) surfaces of Cu, Ag, and Au,[16,17] and recently we have observed a similar surface state on Ni(111).[32] We have observed that the peak at $E_i = -0.4$ eV for Cu(111) normal emission was very sensitive to the condition of the surface, i.e., the intensity was greatly reduced by either adsorbing gases on the surface or by a light Ar-ion sputtering which disordered the surface layer. We do not assign this peak to indirect emission from the L_2' point because of the discrepancy this would give with the experimental bulk band structure arrived at above ($L_2' = -0.9$ eV) and because indirect emission from the L_2' point is identified as a separate structure (the small peak at $E_i \sim -1$ eV for $h\nu = 11.5$ eV in Fig. 1). The Λ_1 symmetry of the surface state is deduced from the dependence of the emission intensity on polarization, as is shown in Fig. 3.

Figure 14 shows an initial energy plot of the surface-state emission as a function of the component of momentum parallel to the surface, obtained by collecting spectra at several small polar angles away from normal emission in a plane containing the $[0\bar{1}1]$ direction. The magnitude of momentum parallel to the surface, k_s, is calculated from

$$k_s = (2mE/\hbar^2)^{1/2} \sin\theta ,$$

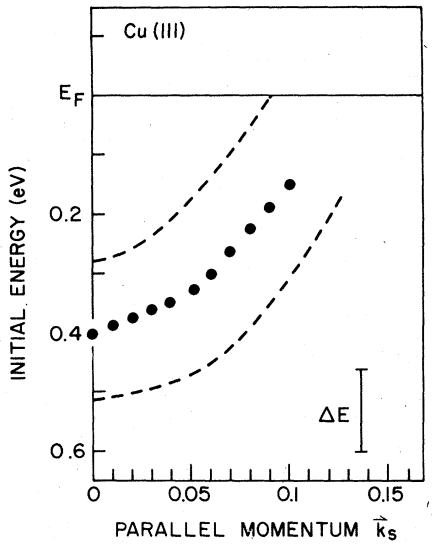

FIG. 14. Experimental energy dispersion of Cu (111) surface-state emission, plotted vs $\vec{k}_s$, the component of momentum parallel to the surface, in units of $k_s/k_{BZ}^{\langle 011\rangle}$, where $k_{BZ}^{\langle 011\rangle}=1.64$ Å^{-1} is the magnitude of k_s at the surface Brillouin-zone corner. The experimental energy resolution is indicated.

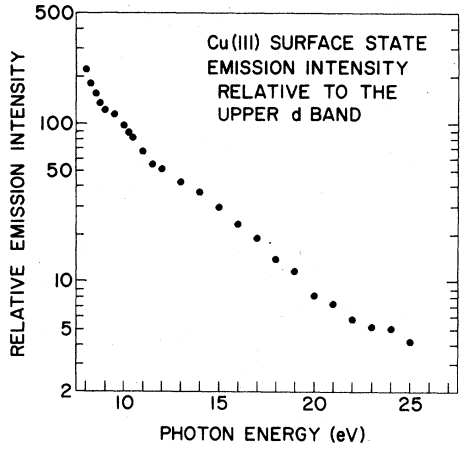

FIG. 15. Relative photoionization cross section for emission from the Cu(111) surface state, plotted vs photon energy.

where E is the measured kinetic energy and θ is the polar angle away from normal emission. The dispersion is to higher energy as k_s moves away from normal emission, as was observed elsewhere.[4] The dots plotted in Fig. 14 are the peak position, while the dotted lines represent the FWHM of the surface state emission. The momentum scale is labeled in fractions of the distance to the corner of the surface Brillouin zone in the $[0\bar{1}1]$ direction, which for Cu(111) is at $k_s=1.641$ Å^{-1}. The instrumental energy resolution (140 meV) for these data, including both photon energy bandwidth (~100 meV) and the analyzer resolution (~100 meV), is indicated by a bar in the figure. Upon correcting for the experimental resolution (~0.15 eV), the estimated intrinsic lifetime broadening of the surface state at $\bar{\Gamma}$ ($E_i=-0.4$ eV) is ~0.2 eV; this is comparable to the d-state broadening at much lower initial energies ($E_i=-2$ eV) and is due to strong s-p electron scattering. Using the display electron spectrometer, we have also directly observed that the dispersion to higher energy is cylindrically symmetric about the surface normal.

The relative photoionization cross section for emission from the surface state, as suggested by Figs. 1 and 2, is a strongly decreasing function of the photon energy. Figure 15 depicts the cross section for the photon energy range $8\leq h\nu\leq 25$ eV. The experimental points represent the intensity of surface-state emission at each photon energy divided by the upper d-band emission at the same photon energy, plotted on a logarithmic scale. This plot of relative emission intensity, while smoothly modulated by the final energy dependence of the upper d-band cross section, suffices to show that there are no apparent resonances in the cross section for surface-state emission over the measured photon energy range. The relative intensity of emission goes down continuously by more than two orders of magnitude between $h\nu=8$ eV and 25 eV. This is consistent with the fact that the oscillator strengths of $3d$-like states decrease slowly for $h\nu\lesssim 100$ eV, while those of sp-like states go down much more rapidly with increasing photon energy.[33]

VII. COMPARISON WITH THEORY AND EXPERIMENT

A summary band diagram of experimentally determined E vs $\vec{k}$ dispersion relations is shown in Fig. 16 for reference, along with the bands from the two-parameter $X\alpha$ calculation.[13] The experimental points along the occupied bands were determined using the calculated Λ_1 and Δ_1 final bands shown in the figure, as described in Sec. III. The experimental E vs $\vec{k}$ points along portions of those same Λ_1 and Δ_1 final bands, on the other hand, were determined by using the uppermost parts of the calculated initial sp band, as described in Sec. IV. The overall agreement between experiment and calculation[13] is remarkable. However, as will be shown in Table I, there is more than one calculation which agrees very well with experiment, notably those by Smith and Mattheiss[22] and Chen and Segall.[34]

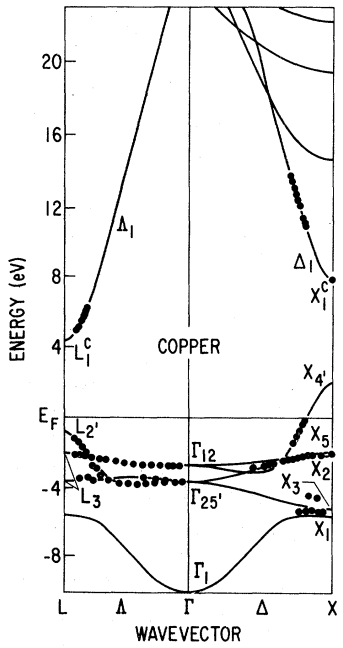

FIG. 16. Energy bands of copper for the two-parameter ($\alpha = 0.77$, $\lambda = 0.08$) self-consistent calculation due to J. F. Janak, A. R. Williams, and V. L. Moruzzi (Ref. 13), together with our experimental E vs $\vec{k}$ dispersion points.

Table I summarizes the energies of selected critical points for occupied bands, as well as two final-band critical points and the width of the $3d$ bands. Values determined in this work together with values determined by many previous representative calculations and experiments are included. The first line presents values derived by the procedures described in Secs. III and IV. The error bounds represent a combination of several factors, including instrumental resolution, angular uncertainties, estimated errors in assigning peak energies, and uncertainties due to broad or weak emission profiles. In addition, the energies of certain points, such as that of the L_2' point, were deduced by interpolation from data which did not probe completely to the zone edge (see Fig. 6). Also, the energy of the X_1^c final-band critical point was determined as shown in Fig. 8, using the overall final density of states and the d-band photoionization cross section. The assignment of the energy position of X_1^c is thus somewhat more uncertain than for the more direct methods of Secs. III and IV.

The first two calculations shown in Table I after the experimental data are due to Janak, Williams, and Moruzzi.[13,20] The first set of energies are from the two-parameter, self-consistent $X\alpha$ calculation ($\alpha = 0.77$, $\lambda = 0.08$) which was fit to various

TABLE I. Experimental and theoretical energy levels for copper (eV relative to E_F).

	L_2'	L_3	L_3	Γ_{12}	$\Gamma_{25'}$	X_5	X_2	X_3	X_1	L_1^c	X_1^c	$X_5 - X_1$
Present work	0.9 ± 0.2	2.25 ± 0.1	3.65 ± 0.1	2.85 ± 0.1	3.65 ± 0.1	2.05 ± 0.1		4.5 ± 0.15	5.2 ± 0.1		7.9 ± 0.2	3.1 ± 0.2
Janak, Williams, and Moruzzi[a]	0.90	2.15	3.68	2.75	3.57	1.95	2.20	5.02	5.50	4.26	7.9	3.55
Janak, Williams, and Moruzzi[b]	0.83	2.0	3.4	2.5	3.28	1.81	2.0	4.62	5.10	3.95	7.2	3.29
Chen and Segall[c]	0.90	2.13	3.65	2.77	3.59	1.96	2.17	4.96	5.46	4.14	7.81	3.50
Burdick[d]	0.61	2.09	3.51	2.69	3.48	1.95	2.12	4.83	5.33	3.95	7.29	3.38
Chodorow[e]	0.61	1.95	3.50	2.79	3.59	1.90	2.19	4.94	5.10			3.20
Segal[f]	0.87	2.68	4.46	3.40	4.38	2.49	2.72	6.08	6.57	1.39	4.79	4.08
Snow[g]	0.39	2.16			3.41	2.03			5.07			3.04
Fong, Walter, and Cohen[h]	0.69	2.30	3.95	3.10	3.85	1.96	2.31	5.20	5.29			3.33
O'Sullivan, Switendick, and Schirber[i]	0.84	2.01			3.28	1.86			5.07	3.97		3.21
Lindau and Wallden[j]	0.75					2.0						
Eastman and Cashion[k]						2.0						3.0 ± 0.3
Becker, Dietz, Gerhardt, and Angermüller[l]	0.87	2.13										

[a] Reference 13.
[b] Reference 20.
[c] Reference 34.
[d] Reference 23.
[e] Reference 35.
[f] Reference 36.
[g] Reference 37.
[h] Reference 38.
[i] Reference 39.
[j] Reference 40.
[k] Reference 41.
[l] Reference 2.

experimental data, including Fermi-surface, optical data, and angle-averaged photoemission.[13] This calculation was used in Secs. III and IV and is shown more completely in Fig. 16. As noted above, the agreement between experiment and this calculation is very good, generally within 0.1 eV, except near the bottom of the d bands at X_3 and X_1. This calculation has d bands which are ~0.4 eV too wide. The second calculation shown for Janak, Williams, and Moruzzi[20] is the same $X\alpha$ calculation as Ref. 13, but without any adjustment to the self-energy ($\lambda = 0$). As noted in Sec. III, this calculation places the d bands ~0.2 eV too high in energy, although the width (3.29 eV) is closer to experiment than the adjusted version. A similar *ab initio* calculation done by Moruzzi *et al.*[21] gives d bands which are shifted upwards by ~0.4 eV compared to experiment.

The next entry in Table I, an empirically adjusted calculation by Chen and Segall,[34] gives excellent agreement with experiment and is generally within less than 0.1 eV of the two-parameter $X\alpha$ calculation.[13] Thus, either of these band structures could have as easily served for the analysis of Secs. III and IV. A similar combined interpolation scheme used by Smith and Mattheiss[22] paid particular attention to fitting the unoccupied bands, in order to more readily interpret angle-averaged photoemission data. The empirical parametrization scheme by Chen and Segall[34] was fit to available Fermi-surface data and several energy gaps determined by optical transitions. There is a fairly large literature on optical data from copper (e.g., see Ref. 34).

The calculation by Burdick[23] used the APW method and a potential originated by Chodorow.[35] This calculation—one of the earliest complete band calculations for copper—shows reasonable agreement with experiment, generally within $\lesssim 0.2$ eV, although the unoccupied bands are less accurate (X_1^c is ~0.6 eV too low). The Chodorow potential[35] which was used in Burdick's calculation was the first reasonable potential devised for copper, and gives a rather good description of the d bands. The original values calculated by Chodorow[35] are also shown in Table I, referenced to a Fermi level determined by Segall.[36] Interestingly, the d-band width agrees well with experiment. The next entry in Table I is that of the earliest complete band calculation of a noble metal, done for copper by Segall[36] using the Green's-function method. Segall calculated the bands using both the Chodorow potential and a more general potential designed to improve the results for states which are s and p in character. The results for this latter potential, shown in Table I, are in rather poor agreement with experiment everywhere but the L_2' point. Snow's results[37] are those of a self-consistent APW calculation (Slater = $\frac{5}{6}$) which gives the correct d-band width but poor agreement at L_2'. Fong, Walter, and Cohen[38] used the empirical-pseudopotential method, and obtained values generally within 0.2–0.3 eV of experiment. O'Sullivan, Switendick, and Schirber[39] used the Korringa-Kohn-Rostoker (KKR) method and a potential derived from Herman-Skillman atomic calculations.

A number of workers have studied angle-averaged photoemission from copper,[40-43] as well as angle-resolved photoemission.[1-9] Energy levels determined by a representative few of these experiments are included in Table I. Many optical and photoemission studies[40,41,44] have deduced that the top of the d bands was 2.0 eV below E_F. Eastman and Cashion[41] and Smith[44] extended their studies to higher photon energies and determined a d-band width of 3.0 (±0.3) eV.

Angle-resolved photoemission from copper was first investigated by Gerhardt and Dietz.[1] Becker *et al.*[2] continued this work and deduced a value for the L_2' point (0.87 eV) which is in agreement with the present work. Ilver and Nilsson[3] studied angle-resolved photoemission at $h\nu = 16.8$ and 21.2 eV and found that they were able to explain all their experimental peaks by use of the direct transition model and the calculation by Janak *et al.*[13] Shirley and co-workers[5-8] have also been successful in applying the direct transition model to explain their angle-resolved photoemission data, obtained at photon energies above 32 eV.

ACKNOWLEDGMENTS

We wish to thank the staff of the University of Wisconsin's Synchrotron Radiation Center, J. J. Donelon and A. Marx, for their capable help. U. Gerhardt is acknowledged for determining the linewidth formula in Sec. V. The storage ring is supported by the National Science Foundation, under Contract No. DMR 77-21888. This paper was supported in part by the Air Force Office of Scientific Research under Contract No. F44620-76-C-0041.

[1]U. Gerhardt and E. Dietz, Phys. Rev. Lett. 26, 1477 (1971).
[2]H. Becker, E. Dietz, U. Gerhardt, and H. Angermüller, Phys. Rev. B 12, 2084 (1975).
[3]L. Ilver and P. O. Nilsson, Solid State Commun. 18, 677 (1976).

[4]P. O. Gartland and B. J. Slagsvold, Phys. Rev. B 12, 4047 (1975).
[5]J. Stöhr, G. Apai, P. S. Wehner, F. R. McFeely, R. S. Williams, and D. A. Shirley, Phys. Rev. B 14, 5144 (1976).
[6]R. S. Williams, P. S. Wehner, J. Stöhr, and D. A. Shirley, Phys. Rev. Lett. 39, 302 (1977).
[7]P. S. Wehner, G. Apai, R. S. Williams, J. Stöhr, and D. A. Shirley, in *Fifth Conference on Vacuum Ultraviolet Radiation Physics*, Montepellier, France, 1977 (unpublished), extended abstract No. 67.
[8]J. Stöhr, P. S. Wehner, R. S. Williams, G. Apai, and D. A. Shirley, Phys. Rev. B 17, 587 (1978).
[9]E. Dietz and U. Gerhardt (unpublished).
[10]H. Y. Fan, Phys. Rev. 68, 43 (1945); L. Apker, E. Taft, and J. Dickey, *ibid.* 74, 1462 (1948); W. E. Spicer, *ibid.* 112, 114 (1958); E. O. Kane, *ibid.* 127, 131 (1962); C. N. Berglund and W. E. Spicer, *ibid.* 136, A1030 (1964).
[11]L. F. Wagner, Z. Hussain, and C. S. Fadley, Solid State Commun. 21, 257 (1977).
[12]N. V. Smith and M. M. Traum, Phys. Rev. Lett. 31, 1247 (1973).
[13]J. F. Janak, A. R. Williams, and V. L. Moruzzi, Phys. Rev. B 11, 1522 (1975).
[14]J. A. Knapp, G. J. Lapeyre, N. V. Smith, and M. M. Traum (unpublished).
[15]E. O. Kane, Phys. Rev. Lett. 12, 97 (1964).
[16]P. Heimann, H. Neddermyer, and H. F. Roloff, J. Phys Phys. C 10, 473 (1978).
[17]G. V. Hansson and S. A. Flodström, Phys. Rev. B 17, 473 (1978).
[18]J. Hermanson, Solid State Commun. 22, 9 (1977).
[19]C. R. Brundle, Surf. Sci. 48, 99 (1975); I. Lindau and W. E. Spicer, J. Electron. Spectrosc. 3, 409 (1974); C. J. Powell, Surf. Sci. 44, 29 (1974).
[20]J. F. Janak, A. R. Williams, and V. L. Moruzzi, Phys. Rev. B 6, 4367 (1972).
[21]V. L. Moruzzi, A. R. Williams, and J. F. Janak, *Calculated Electronic Properties of Metals* (Pergamon, New York, 1978).
[22]N. V. Smith and L. F. Mattheiss, Phys. Rev. B 9, 1341 (1974).
[23]G. A. Burdick, Phys. Rev. 129, 138 (1963).
[24]E. O. Kane, Phys. Rev. 127, 131 (1962).
[25]D. E. Eastman, J. A. Knapp, and F. J. Himpsel, Phys. Rev. Lett. 41, 825 (1978).
[26]For example, see J. Pendry, in *Photoemission and the Electronic Properties of Surfaces* (Wiley, New York, 1978).
[27]H. Kantor, Phys. Rev. B 1, 2357 (1970).
[28]D. E. Eastman (unpublished).
[29]D. Norman and D. P. Woodruff, Surf. Sci. (to be published).
[30]P. W. Palmberg and T. N. Rhodin, J. Appl. Phys. 39, 2425 (1968).
[31]J. E. Demuth, P. M. Marcus, and D. W. Jepsen, Phys. Rev. B 11, 1460 (1975).
[32]F. J. Himpsel and D. E. Eastman, Phys. Rev. Lett. 41, 507 (1978).
[33]D. E. Eastman in *Proceedings of the Fourth International Conference on* VUV *Physics*, *Hamburg*, *1974* (Pergamon, Vieweg, 1974), p. 417.
[34]An-Ban Chen and B. Segall, Phys. Rev. B 12, 600 (1975).
[35]M. Chodorow, Phys. Rev. 55, 675 (1939); Ph.D. thesis (Massachusettes Institute of Technology, 1939) (unpublished).
[36]B. Segal, Phys. Rev. 125, 109 (1962).
[37]E. C. Snow, Phys. Rev. 171, 785 (1968).
[38]C. Y. Fong, J. P. Walter, and M. L. Cohen, Phys. Rev. B 11, 2759 (1975).
[39]W. J. O'Sullivan, A. C. Switendick, and J. E. Schirber, Phys. Rev. B 1, 1443 (1970).
[40]I. Lindau and L. Walldén, Phys. Scr. 3, 77 (1971).
[41]D. E. Eastman and J. K. Cashion, Phys. Rev. Lett. 24, 310 (1970).
[42]C. N. Berglund and W. E. Spicer, Phys. Rev. 136, A1030 (1964); 136, A1044 (1964).
[43]N. V. Smith, Phys. Rev. Lett. 23, 1452 (1969).
[44]N. V. Smith, Phys. Rev. B 3, 1862 (1971).